Polyoxometalate-Encapsulated Twenty-Nuclear Silver-tetrazole Nanocage Frameworks as Highly Active Electrocatalysts for the Hydrogen Evolution Reaction

Shaobin Li,[a,b†] Li Zhang,[a†] Yaqian Lan[c], Kevin P. O'Halloran[d], Huiyuan Ma,[a*] and Haijun Pang[a*]

[a]*Key Laboratory of Green Chemical Engineering and Technology of College of Heilongjiang Province, College of Chemical and Environmental Engineering, Harbin University of Science and Technology, Harbin 150040, P. R. China. E-mail: mahy017@163.com (Ma H. Y.), panghj116@163.com (Pang H. J.).*

[b]*Key Laboratory of Polymeric Composite Materials of Heilongjiang Province, College of Materials Science and Engineering, Qiqihar University, Qiqihar 161006, P. R. China.*

[c]*College of Chemistry and Materials Science, Nanjing Normal University, Nanjing 210023, P. R. China.*

[d]*School of Science and Technology, Georgia Gwinnett College, Lawrenceville, GA 30043, USA.*

† These authors contributed equally to this work.

Table of contents:

Section 1 Experimental Section

I. Materials and General Methods

All other reagents were purchased commercially and were used without further purification. Elemental analyses (C, H and N) were performed on a Perkin-Elmer 2400 CHN Elemental Analyzer, and that of Ag, W were carried out with a Leaman inductively coupled plasma (ICP) spectrometer. The FT-IR spectra were recorded from KBr pellets in the range of 4000–400 cm^{-1} with a Nicolet AVATAR FT-IR360 spectrometer. The powder X-ray diffraction (PXRD) data were collected on a Rigaku RINT 2000 diffractometer at room temperature.

II. Synthesis of HUST-100

A mixture of $H_3PW_{12}O_{40}$ (0.35 g, 0.072 mmol), $AgNO_3$ (0.15 g, 0.6 mmol), tta (0.072 g, 0.38 mmol) and 1,3,5-benzenetricarboxylate (0.072 g, 0.38 mmol) were dissolved in 15 mL of distilled water at room temperature. After the pH value of the mixture was adjusted to about 2.5 with 3.0 M HNO_3, the suspension was put into a Teflon-lined autoclave and kept under autogenous pressure at 170 °C for 5 days. After slow cooling to room temperature, red block crystals of **1** were filtered, washed with distilled water and dried at room temperature. Yield: 47 % (based on W). The final pH value of the solution after the reaction is approximately 2.3. The reproducibility of **HUST-100** is good. Anal. calc. for $C_4H_{12}N_{16}O_{44}PW_{12}Ag_{10}$: Calc.: C, 1.12; H, 0.28; N, 5.21; P, 0.72; W, 51.25; Ag, 25.06 %; Found: C, 1.08; H, 0.31; N, 5.26; P, 0.71; W, 51.32; Ag, 25.12 %.

Synthesis of HUST-101

The synthetic method was similar to that of **HUST-100**, except that $H_3PW_{12}O_{40}$ was replaced by $H_4SiW_{12}O_{40}$. Red block crystals of **HUST-101** were filtered, washed with water, and dried at room temperature. Yield: 49 % (based on W). The final pH value of the solution after the reaction is approximately 2.3. The reproducibility of **HUST-101** is good. Anal. calc. for $C_4H_{12}N_{16}O_{44}SiW_{12}Ag_{10}$: Calc.: C, 1.12; H, 0.28; N, 5.21; Si, 0.65; W, 51.29; Ag, 25.08 %; Found: C, 1.09; H, 0.30; N, 5.25; Si, 0.69; W, 51.34; Ag, 25.13 %.

III. Preparation of Working Electrodes. A mixture of 20 mg of carbon black (Vulcan XC-72R) and the desired amount of as-synthesized samples was co-grounded for 45 min. Prior to be modified, the GCE was polished carefully with 0.05 μm alumina powders and then cleaned with HNO_3 (1:1), ethanol, and deionized water, respectively. Catalyst ink was prepared by mixing 5 mg of the prepared catalyst powders into water (950μL) containing 0.5 wt % Nafion (50 μL) and then ultrasonically dispersed for 30 min. Then, an aqueous dispersion was transferred onto the washed GCE (5μL) and dried in air at room temperature before electrochemical experiments.

IV. Electrochemical Measurements. Cyclic voltammetry (CV) and linear sweep voltammetry (LSV) tests were conducted with a CHI760E workstation in a conventional three electrode system. A modified GCE (d = 3 mm) served as the working electrode in electrochemical experiments, a platinum wire as the counter

electrode, and an Ag/AgCl electrode as the reference electrode, respectively. For parallel comparison with literature values, the potential vs. Ag/AgCl was converted to reversible hydrogen electrode (RHE) according to the Nernst equation: E(RHE) = E(Ag/AgCl) + 0.059 pH + 0.205 V. Linear sweep voltammetry (LSV) is conducted from 0 to −1.0 V with a scan rate of 5 $mV \cdot s^{-1}$. The working electrode was blown using a steady N_2 flow to remove hydrogen gas bubbles formed at the catalyst surface. The durability tests were carried out by repeating the potential scan from 0.4 to −0.6 V at a scan rate of 100 $mV \cdot s^{-1}$ for 2000 cycles. Electrochemical impedance spectroscopy (EIS) was carried out from 10 kHz to 0.01 Hz with an amplitude of 5 mV at the open-circuit voltage.

V. Single Crystal X-ray Crystallography

Single crystal X-ray diffraction data collection of **HUST-100** and **HUST-101** were performed using a Bruker Smart Apex CCD diffractometer with Mo-*Ka* radiation (λ = 0.71073 Å) at 293 K. Absorption correction was applied by using the multi-scan program SADABS.[1] The structure was solved by the direct method, and non-hydrogen atoms were refined anisotropically by least-squares on F^2 using the SHELXTL program.[2] The hydrogen atoms of organic ligands were generated geometrically for **HUST-100** and **HUST-101**, while the hydrogen atoms of water molecules can not be found from the residual peaks, they were included in the final molecular formula. A summary of the crystal data, data collections and refinement parameters for **HUST-100** and **HUST-101** are listed in Table S1 and the selected

bond lengths and angles are given in Table S2. Crystallographic data for the structures reported in this paper have been deposited in the Cambridge Crystallographic Data Center with CCDC Number: 1588388 and 1588233 for **HUST-100** and **HUST-101**, respectively.

Table S1 Crystal data and structure refinements for **HUST-100** and **HUST-101**.

Compound	**HUST-100**	**HUST-101**
Formula	$C_4H_{12}Ag_{10}N_{16}O_{44}PW_{12}$	$C_4H_{12}Ag_{10}N_{16}O_{44}SiW_{12}$
Formula weight	4303.98	4301.10
Crystal system	Tetragonal	Tetragonal
Space group	*I4m2*	*I4m2*
a/Å	14.182(5)	14.198(5)
b/Å	14.182(5)	14.198(5)
c/Å	12.331(5)	12.297(5)
α/°	90	90
β/°	90	90
γ/°	90	90
V/Å^3	2480(2)	2479(2)
Z	2	2
D_{calcd}/g cm^{-3}	5.753	5.751
T/K	293(2)	293(2)
μ/mm^{-1}	31.694	31.698
Refl. Measured	9219	9241
Refl. Unique	1690	1692
R_{int}	0.0311	0.0408
F(000)	3730.0	3728.0
GoF on F^2	0.819	1.098
R_1/wR_2 [$I \geq 2\sigma(I)$]	0.0441/0.1228	0.0367/0.0971

$$R_1 = \sum \| F_o | - | F_c \| / \sum | F_o | \,.\; wR_2 = \sum [w(F_o^2 - F_c^2)^2] / \sum [w(F_o^2)^2]^{1/2}$$

Table S2 The selected bond lengths (Å) and angles (°) for **HUST-100** and **HUST-101**.

		HUST-100	
W(1)-O(1)	1.675(17)	W(1)-O(2)#1	1.909(12)
W(1)-O(2)	1.909(12)	W(1)-O(7)#2	2.421(16)
W(2)-O(3)	1.888(4)	W(2)-O(5)	1.909(8)
O(7)-P(1)	1.541(16)	P(1)-O(7)#2	1.541(16)
Ag(1)-N(1)	2.157(14)	Ag(2)-N(2)	2.303(14)

Ag(1)-O(6)	2.586(12)	O(1)-Ag(3)	2.395(18)
O(1)-W(1)-O(2)#1	102.5(6)	O(2)#1-W(1)-O(6)#2	156.6(6)
O(4)-W(2)-O(2)	102.3(5)	O(3)-W(2)-O(2)	86.1(6)
O(4)-W(2)-O(5)	100.6(6)	O(4)-W(2)-O(6)	100.5(6)
O(2)-W(2)-O(6)	87.6(5)	W(2)-O(2)-W(1)	148.9(7)
N(1)-Ag(1)-O(6)	100.0(5)	P(1)-O(7)-W(1)#2	125.4(9)
O(8)#1-Ag(3)-O(8)	72.7(4)	P(1)-O(7)-W(2)	125.5(5)
		HUST-101	
W(1)-O(2)	1.703(10)	W(1)-O(3)	1.892(3)
W(1)-O(1)	1.917(7)	W(1)-O(6)#1	1.914(10)
Si(1)-O(4)#1	1.627(14)	Si(1)-O(4)	1.627(14)
W(2)-O(8)	1.702(14)	W(2)-O(5)	1.899(9)
W(2)-O(4)#1	2.344(13)	W(2)-O(6)	1.934(10)
Ag(2)-O(8)	2.348(16)	Ag(1)-N(3)	2.158(11)
Ag(1)-O(6)	2.572(10)	Ag(3)-N(1)	2.301(12)
O(2)-W(1)-O(3)	101.6(6)	O(2)-W(1)-O(5)	101.4(5)
O(2)-W(1)-O(6)#1	100.0(5)	O(3)-W(1)-O(6)#1	158.2(5)
O(2)-W(1)-O(4)	170.4(5)	O(1)-W(1)-O(4)	74.0(4)
O(4)#1-Si(1)-O(4)	109.5(5)	O(4)-Si(1)-O(4)#2	109.5(5)
O(8)-W(2)-O(6)	100.2(5)	O(8)-W(2)-O(4)#1	169.7(7)
N(3)-Ag(1)-O(6)	100.3(4)	O(6)-Ag(1)-O(6)#3	125.2(5)
N(1)#10-Ag(3)-N(1)	128.6(6)	N(3)-Ag(1)-O(6)#2	84.4(4)

Symmetry transformations used to generate equivalent atoms: #1 x,-y+1,z #2 y,x,-z+2 #3 y,-x+1,-z+2.

Section 2 Supplementary Structural Information

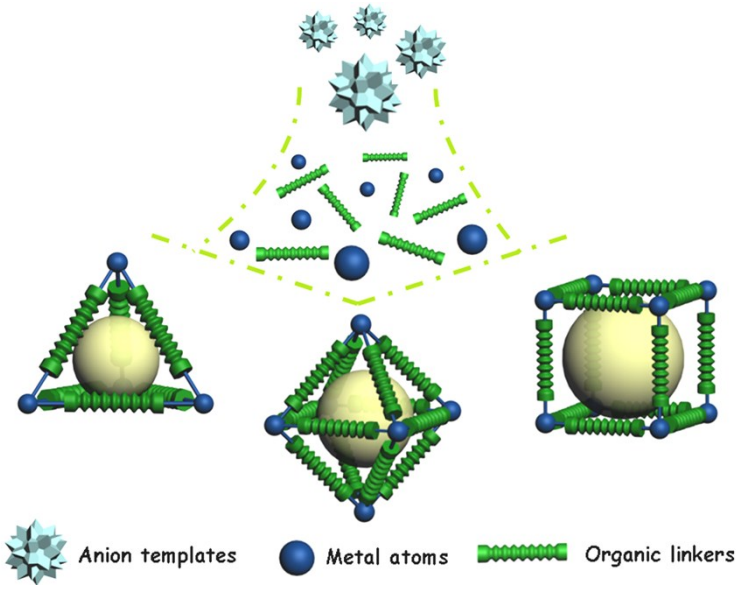

Scheme S1 The schematic synthesis strategy of anions as templates to direct formation of various MONCs.

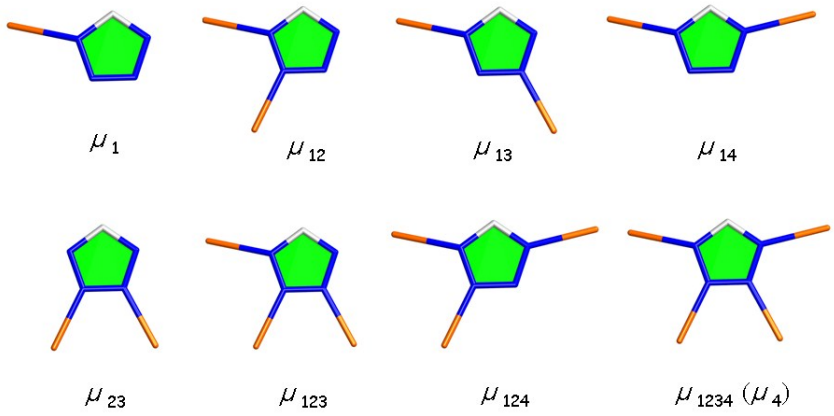

Scheme S2 The potential coordination modes of tta ligands.

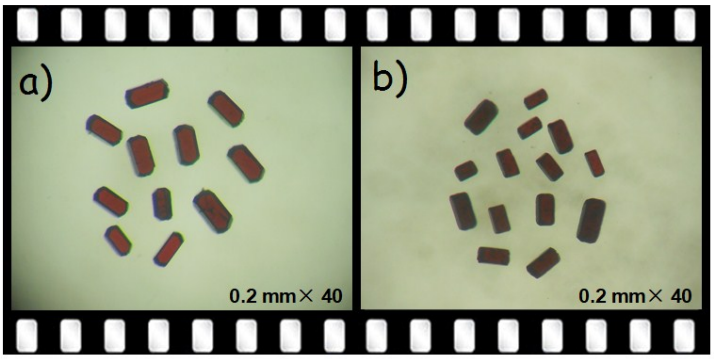

Fig. S1 The images of **HUST-100** (a) and **HUST-101** (b) under an optical microscope with magnified 40 times.

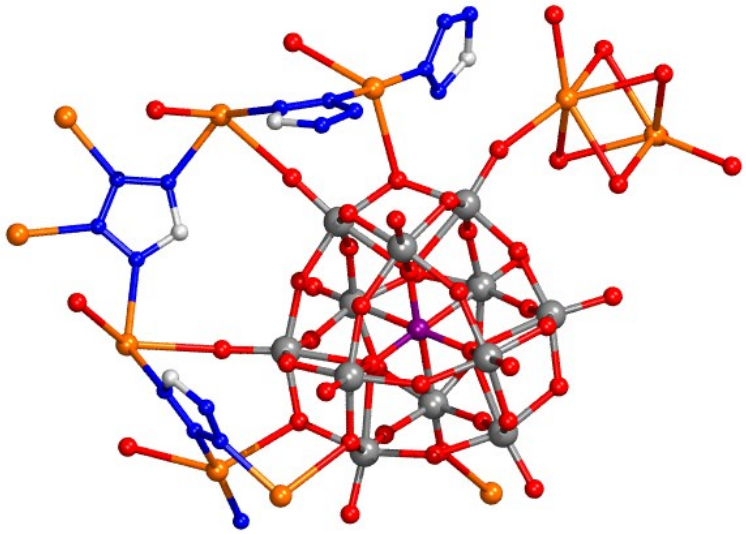

Fig. S2 View of the basic crystallographic unit in **HUST-100** (All the hydrogen atoms are omitted for clarity).

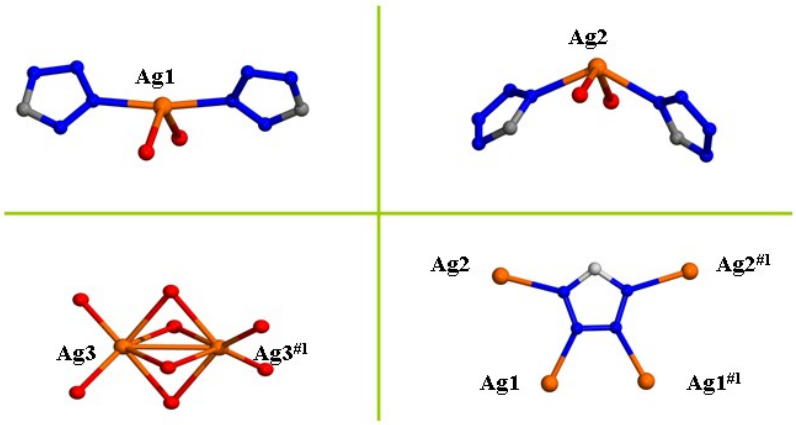

Fig. S3 The coordination modes of three crystallographically-independent Ag cations and tta ligand in **HUST-100**.

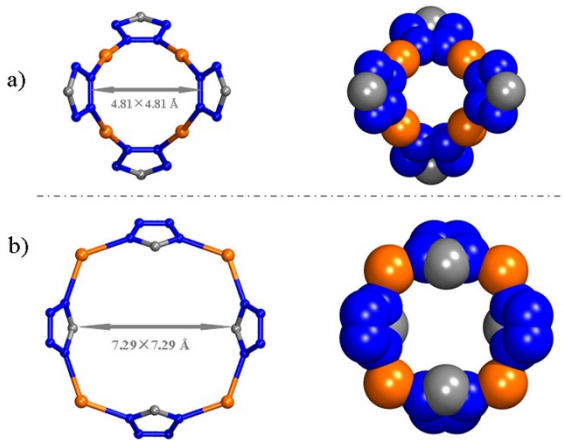

Fig. S4 The macrocycle A (a) and macrocycle B (b) in **HUST-100**.

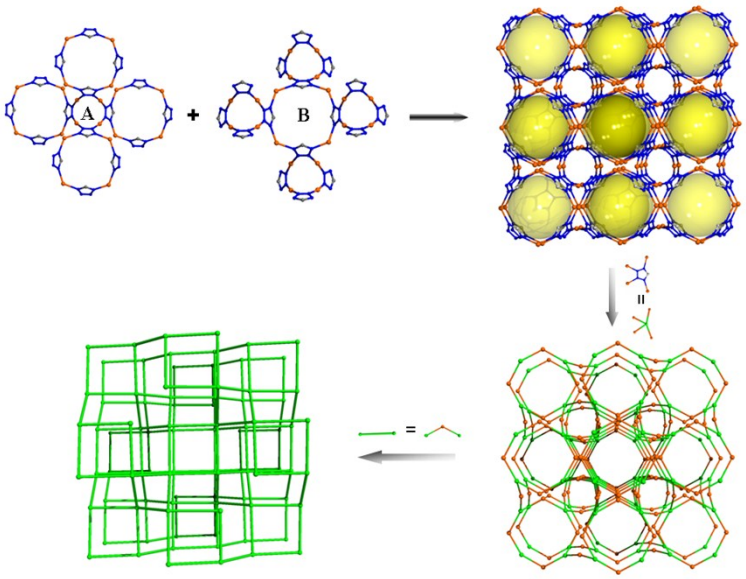

Fig. S5 The illustration of the 3D host MONC framework with a topology of classical ***dia*** net.

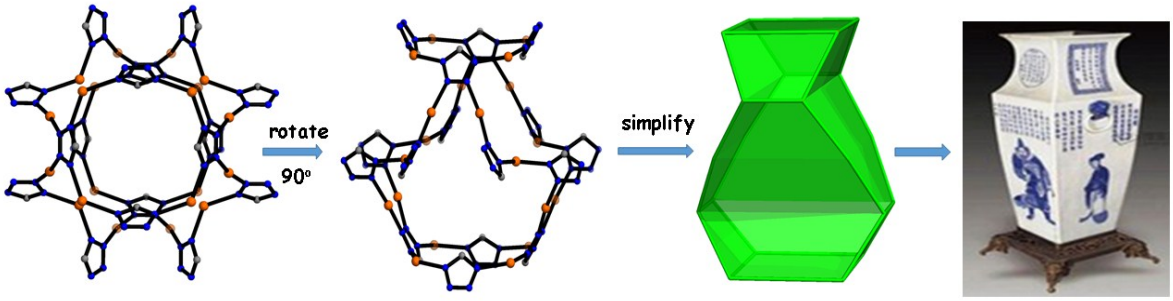

Fig.S6 Illustration of vase-like nanocage.

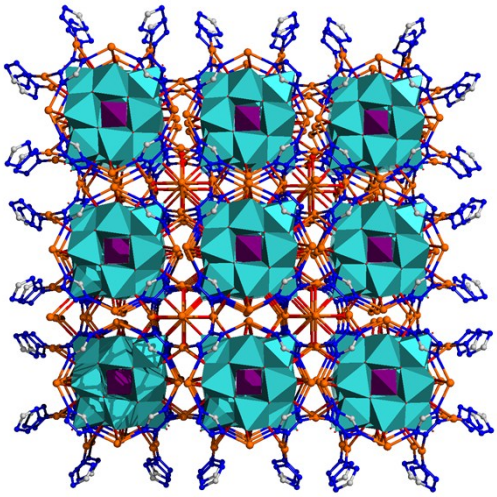

Fig.S7 The 24-connected structure of **HUST-100**.

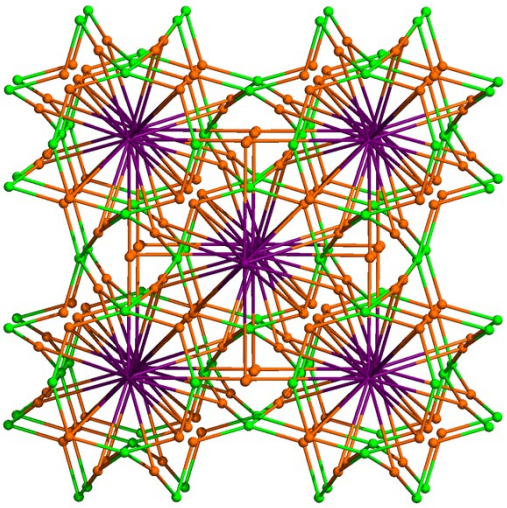

Fig.S8 The 24-connected structure topology of **HUST-100**.

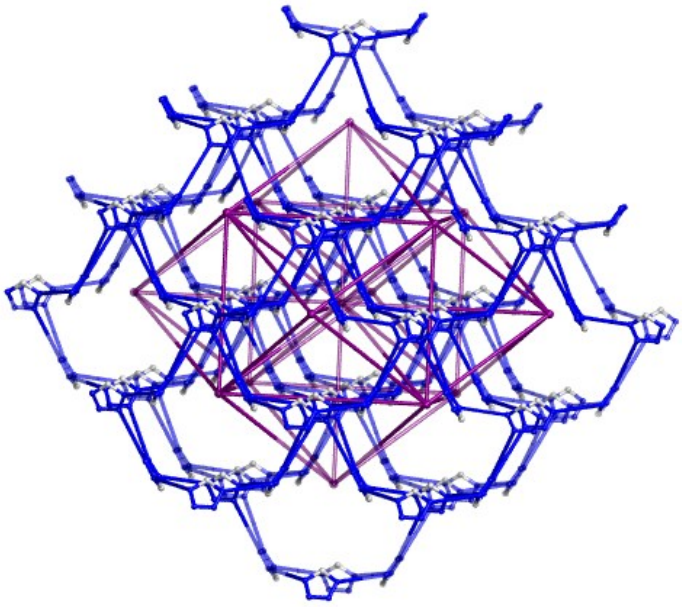

Fig.S9 The connected geometry of adjacent POM-encapsulated $[Ag_{20}(tta)_{16}]^{4+}$ nanocages.

Section 3 Supplementary Physical Characterizations

I. Analyses of BVS, XPS, IR and PXRD measurements

BVS and XPS: HUST-100 and **HUST-101** were synthesized under hydrothermal conditions. All silver atoms are in the +I oxidation state, confirmed by BVS calculations.[3] The XPS spectra of **HUST-100** and **HUST-101** show two overlapping peaks at 35.18 eV and 37.35 eV, 35.12 eV and 37.21 eV, respectively (Fig. S9), which are attributed to W^{V} and W^{VI}.[4] All of these results are consistent with the structural analyses and charge balance.

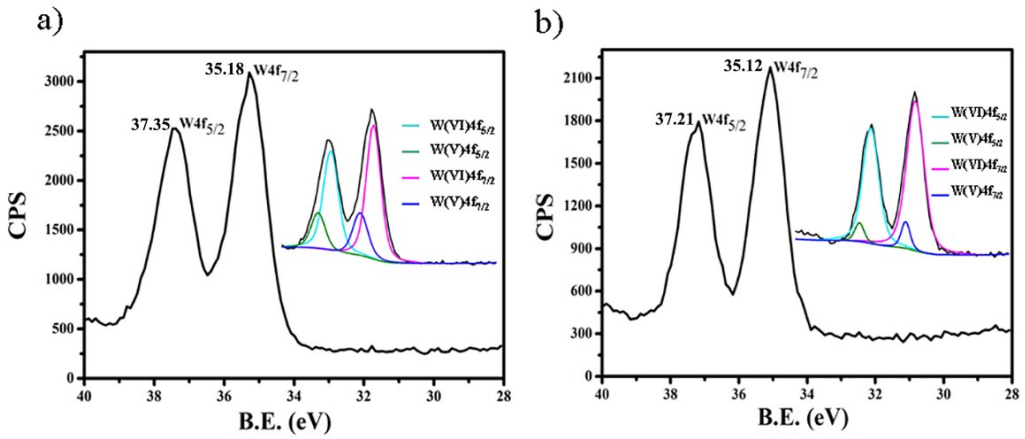

Fig.S10 The XPS analysis of W element in **HUST-100** (a) and **HUST-101** (b), respectively.

IR: The IR spectra exhibit the characteristic peaks at 1036, 937, 873 and 740 cm^{-1} in **HUST-100**, 1021, 931, 882 and 734 cm^{-1} in **HUST-101**, which are attributed to ν(P–O), ν(W=Ot), ν_{as}(W–Ob–W) and ν_{as}(W–Oc–W) from PW_{12} clusters,[5] ν(Si–O), ν(W=Ot), ν_{as}(W–Ob–W) and ν_{as}(W–Oc–W) from SiW_{12} clusters,[6] respectively. Additionally, the bands in the region of 1638–1151 cm^{-1} could be ascribed to the characteristic peaks of tta ligands in **HUST-100** and **HUST-101**.[7] Furthermore, **HUST-100** and **HUST-101** are stable in acidic aqueous solutions in the pH range of 1-7 at room temperature, as confirmed by the IR measurements (Fig. S11).

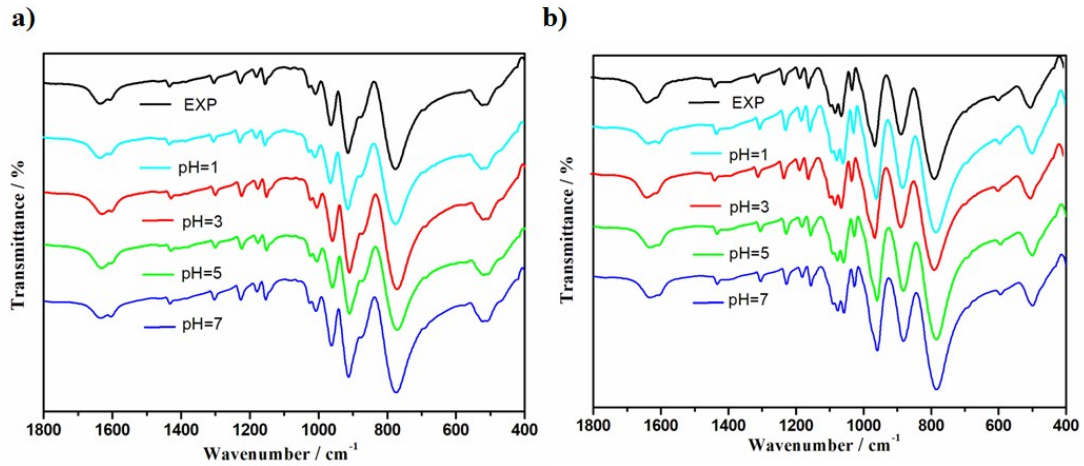

Fig.S11 The IR curves of **HUST-100** (**a**) and **HUST-101** (**b**) immersed in water at room temperature for 48 h at different pH. **Exp** represents the pattern of as-synthesized samples.

PXRD: As shown in Figure S12, the X-ray powder diffraction patterns measured for the as-synthesized samples (placed in the air several months) of **HUST-100** and **HUST-101** are all in good agreement with the PXRD patterns simulated from the respective single-crystal X-ray data, indicating the purity of the bulk phases. Furthermore, **HUST-100** and **HUST-101** are stable in acidic aqueous solutions (soaked for 48 hours) in the pH range of 1-7 at room temperature, as confirmed by the PXRD measurements (Fig. S12). As shown in Fig. S12, the diffraction peaks of simulated and experimental patterns match well in key peaks, however, there is some small change of the peaks in XRD pattern after the mentioned treatment, such as peaks at ~25° (**HUST-100**) and peaks at ~16° (**HUST-101**). This phenomenon may be just ascribed to that the fresh crystals had been deposited for long time and might be partly pulverized after iterativing soaked in acidic aqueous solutions. As is known, the calculated powder patterns are obtained by an ideal single crystal, but the experimental powder patterns are gained by the many identical crystal powders. Hence, the intensity of two kinds of powder patterns is slightly different, especially for the pulverized samples after the mentioned treatment. This phenomenon is similar to the reported literature[8]. In all, the stabilization of **HUST-100** and **HUST-101** is well in acidic aqueous solutions. This result can be further confirmed by IR measurements (Fig. S11) and I-T curves (Fig. S13).

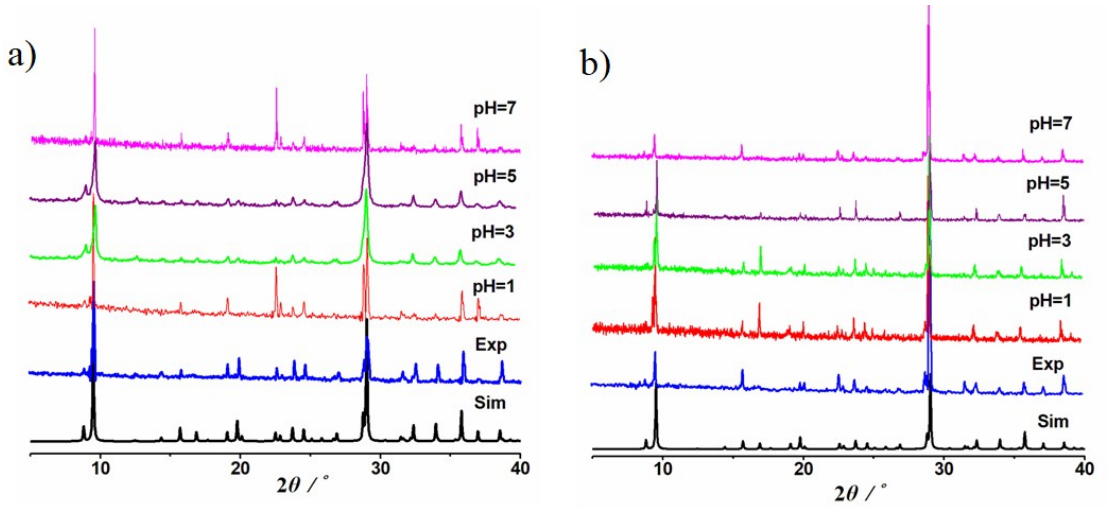

Fig.S12 The PXRD patterns of **HUST-100** (**a**) and **HUST-101** (**b**) immersed in water at room temperature for 48 h at different pH. **Sim** represents the simulated pattern and **Exp** represents the pattern of as-synthesized sample, respectively.

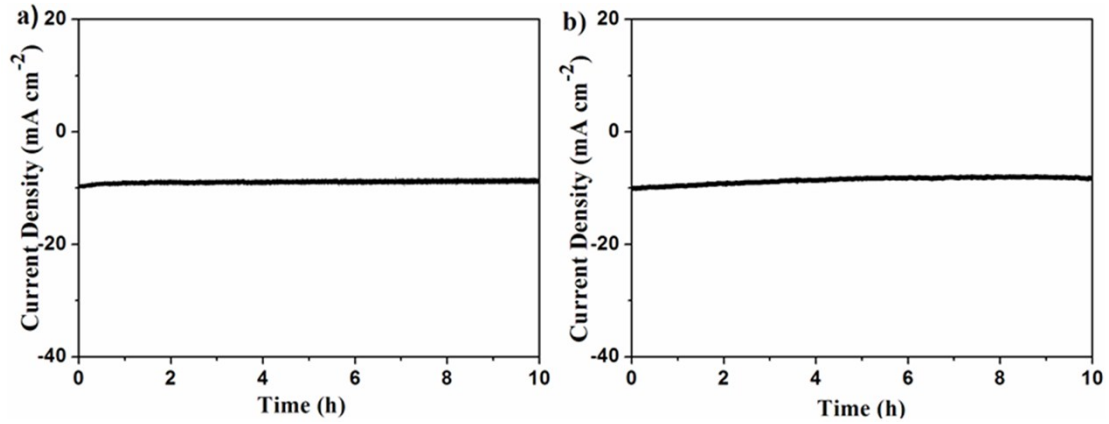

Fig.S13 Time-dependent current density curves (I-T curves) under a static overpotential of 234 mV **HUST-100** (**a**) and 263 mV **HUST-101** (**b**) for 10 h.

Table S3. Comparison of HER activity for reported MOF composite catalysts.

catalyst	onset potential (mV)	η_{10} (mV)	Tafel slope (mV·dec^{-1})	j_0 (A·cm^{-2})	R^2	Ref.
HUST-100	148	234	82	1.1×10^{-5}	0.99739	This work
HUST-101	164	263	94	1.4×10^{-5}	0.99804	
NENU-500	180	237	96	3.6×10^{-5}	0.99982	[9]
NENU-501	304	392	137	1.5×10^{-5}	0.99982	
ε(trim)4/3	420	515	142	2.4×10^{-6}	0.99989	
NENU-499	452	570	122	3.7×10^{-7}	0.99957	

NENU-5	518	585	94	6.1×10^{-9}	0.99986
HKUST-1	612	691	127	3.6×10^{-8}	0.99966

References

1. G. M. Sheldrick, *SADABS 2.05*; University of Göttingen: Göttingen, Germany.

2. *SHELXTL 6.10*; Bruker Analytical Instrumentation: Madison, WI, 2000.

3. I. D. Brown and D. Altermatt, *Acta Crystallogr. Sect. B*., 1985, **41**, 244−247.

4. M. G. Liu, P. P. Zhang, J. Peng, H. X. Meng, X. Wang, M. Zhu, D. D. Wang, C. L. Meng and K. Alimaje, *Cryst. Growth Des*., 2012, **12**, 1273−1281.

5. H. J. Pang, J. C. J. Zhang, Y. G. Li, P. P. Zhang, H. Y. Ma and Z. M. Su, *Chem. Commun*., 2010, **46**, 5097−5099.

6. X. L. Wang. H. L. Hu, G. C. Liu, H. Y. Lin and A. X. Tian, *Chem. Commun*., 2010, **46**, 6485−6487.

7. D. C. Zhong, W. G. Lu, L. Jiang, X. L. Feng and T. B. Lu, *Cryst. Growth Des*., 2010, **10**, 739−746.

8. W. L. Chen, Y. G. Li, Y. H. Wang, E. B. Wang, *Eur. J. Inorg. Chem*. 2007, **2007**, 2216−2220.

9. J. S. Qin, D. Y. Du, W. Guan, X. J. Bo, Y. F. Li, L. P. Guo, Z. M. S, Y. Y. Wang, Y. Q. Lan and H. C. Zhou, *J. Am. Chem. Soc*., 2015, **137**, 7169−7177.